Particle-based simulation of powder application in additive manufacturing

Eric J. R. Parteli, Thorsten Pöschel

Lehrstuhl für Multiscale Simulation, Friedrich-Alexander-Universität Erlangen-Nürnberg, Nägelsbachstr. 49b, 91052 Erlangen, Germany

Abstract

The development of reliable strategies to optimize part production in additive manufacturing technologies hinges, to a large extent, on the quantitative understanding of the mechanical behavior of the powder particles during the application process. Since it is difficult to acquire this understanding based on experiments alone, a particle-based numerical tool for the simulation of powder application is required. In the present work, we develop such a numerical tool and apply it to investigate the characteristics of the powder layer deposited onto the part using a roller as the coating system. In our simulations, the complex geometric shapes of the powder particles are taken explicitly into account. Our results show that increasing the coating speed leads to an increase in the surface roughness of the powder bed, which is known to affect part quality. We also find that, surprisingly, powders with broader size distributions may lead to larger values of surface roughness as the smallest particles are most prone to form large agglomerates thus increasing the packing's porosity. Moreover, we find that the load on the part may vary over an order of magnitude during the coating process owing to the strong inhomogeneity of inter-particle forces in the granular packing. Our numerical tool can be used to assist — and partially replace — experimental investigations of the flowability and packing behavior of different powder systems as a function of material and process parameters.

Key words: Additive manufacturing, numerical simulation, Discrete Element Method

1. Introduction

Additive manufacturing can provide substantial benefits for part production in a broad range of applications compared to conventional machining (Campbell et al., 2012). By selectively melting layers of powder particles, parts of nearly arbitrarily complex geometries can be built directly from a three-dimensional (CAD) model (Heinl et al., 2007; Wendel et al., 2008; Goodridge et al., 2012; Karunakaran et al., 2012; Wudy et al., 2014).

However, there are important open issues that need to be addressed in order to make this technology applicable for large-scale production (Campbell et al., 2012). In particular, the macroscopic characteristics of the produced part, such as porosity, are largely dictated by the geometric properties of the applied powder bed, which in turn depend on the mechanical behaviour of the granular material during the coating process. The quantitative understanding of this behavior is, thus, one essential pre-requisite for developing optimization routes towards improved part quality and shorter production time (Abdel Ghany and Moustafa, 2006; Wendel et al., 2008). Indeed, this behavior depends not only on the process parameters and the mechanical properties of the material constituting the particles, but also on the complex geometric shape of the individual powder particles.

Therefore, in order to reliably describe the mechanical behavior of the powder system during the additive manufacturing process, a *particle-based* numerical simulation tool, which accounts for a physical model for inter-particle forces as well as for a representation of the complex geometric shapes of the constituent particles, is required. In the present work, we develop such a numerical tool, based on the Discrete Element Method (DEM). We will show that our numerical tool can be useful to investigate geometric and dynamic aspects of the powder system employed in the manufacturing process, that are inaccessible to or difficult to investigate by means of experimental measurements. In particular, we focus on the application process using a roller as coating device, and we investigate the forces within the granular system emerging during the transport process, as well as the surface roughness of the deposited powder bed as a function of process speed.

2. Numerical experiments

The powder application process is simulated using the Discrete Element Method, that is, simulatenously solving Newton's equations of translational and rotational motion for all contituent particles of the powder (Gallas and Sokołowski, 1993; Pöschel and Buchholtz, 1993; Herrmann, 1993; Schäfer et al., 1996; Silbert et al., 2001; Zhang and Makse, 2005; Pöschel and Schwager, 2005).

2.1. Model for the complex particles' geometric shapes

One challenge that needs to be addressed for the simulation of the application process is the modeling of parti-

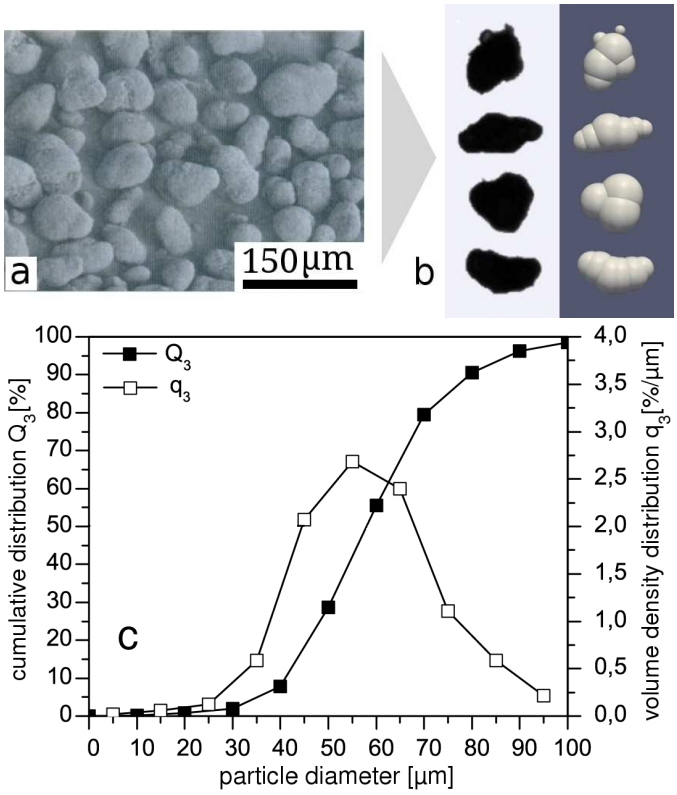

Figure 1: (a) commercially available PA12 powder particles of complex geometric shapes; (b) light microscope images of some of the powder particles (first column) and corresponding particle models using the multisphere method (second column) for implementation in the DEM. (c) cumulative distribution Q_3 and volume density distribution q_3 as a function of the particle diameter (courtesy of Maximilian Drexler, Lehrstuhl für Kunststofftechnik, Friedrich-Alexander-University of Erlangen-Nuremberg).

cle shape. Fig. 1a shows an image of commercially available PA12 (Rietzel et al., 2011) powder particles used in the manufacturing process through selective laser melting (Wudy et al., 2014). As we can see, these particles display a diversity of geometric shapes that strongly differ from the round one. This can be also seen in the light microscope images displayed in the left column of Fig. 1b. It is well-known that granular systems constituted of non-spherical particles behave differently from particulate systems composed of spherical particles (Pöschel and Schwager, 2005). Therefore, the accurate representation of the particle shape is indispensable for the reliable simulation of powder application in additive manufacturing.

The complex geometric shape of powder particles is modeled here by means of the multisphere method, which consists of combining spherical particles of different sizes to approximate the non-spherical shape (Gallas and Sokołowski, 1993; Pöschel and Buchholtz, 1993; Kruggel-Emden et al., 2008; Garcia et al., 2009; Ferellec and McDowell, 2010; Parteli, 2013). In this method, each composite particle leads to a rigid body of complex geometric shape, the total force on which is computed by summing up the forces on all constituent spheres. Moreover, the resulting angular momentum of the complex particle is obtained from the total torque on all spheres with respect to the body's center of mass (see e.g. Kruggel-Emden et al. (2008)). The right column in Fig. 1b shows images of composite particles constructed with the multisphere method in order to approximate the corresponding particle shapes displayed in the light microscope images.

However, in order to apply the multisphere method for the simulation of particles of complex geometric shapes, the moment of inertia of the composite particle must be correctly calculated. As a matter of fact, each such particle is constituted of small beads of different sizes, which may overlap or not depending on the particle shape modelled with the multisphere method. The beads constituting a given complex particle do not interact with each other, that is the interaction forces — described below — are not computed for pairs of beads within the same complex particle. In our simulations, we compute the mass and the moment of inertia of each complex particle by explicitly removing the contribution due to the overlap volumes between constituent spheres, using a recently derived model (Parteli, 2013).

2.2. Model for the inter-particle forces

The interactions between spherical particles belonging to distinct composite particles are calculated by considering both contact forces and attractive particle interaction forces (Pöschel and Schwager, 2005; Parteli et al., 2014).

The contact forces in DEM simulations can be described using a variety of models, each of which is suitable for a particular particle geometry and material behavior. Reviews of these models have been presented, for instance, by Schäfer et al. (1996); Pöschel and Schwager (2005); Kruggel-Emden et al. (2007, 2008). In our simulations, we assume viscoelastic interaction in normal direction Brilliantov et al. (1996) and employ a modified Cundall-Strack model (Cundall and Strack, 1979) for computing the tangential component of the contact force (Cundall and Strack, 1979). The normal and tangential components of the contact forces read,

$$\vec{F}_n = \min\left(0, -\rho\xi^{3/2} - \frac{3}{2}A_n\rho\sqrt{\xi}\dot{\xi}\right)\vec{e}_n\,, \tag{1}$$

$$\vec{F}_t = -\min\left[\mu\left|\vec{F}_n\right|, \int_{\text{path}}\frac{4G}{2-\nu}\sqrt{R_{\text{eff}}\xi}\,\mathrm{d}s + A_t\sqrt{R_{\text{eff}}\xi}v_{\text{t}}\right]\vec{e}_t, \tag{2}$$

where

$$\xi = R_1 + R_2 - |\vec{r}_1 - \vec{r}_2| \tag{3}$$

is the compression of colliding particles, which have radii R_1 and R_2 and are at positions $\vec{r}_1$ and $\vec{r}_2$.

In Eq. (1), $\vec{e}_n \equiv (\vec{r}_1 - \vec{r}_2)\,/\,|\vec{r}_1 - \vec{r}_2|$ is the normal unit vector. Moreover, the elastic parameter ρ is a function

of the the effective radius $R_{\rm eff} \equiv R_1 R_2/(R_1 + R_2)$, the Young's modulus, Y, and the Poisson's ratio ν,

$$\rho \equiv \frac{2Y}{3(1-\nu^2)}\sqrt{R_{\rm eff}}. \tag{4}$$

while the dissipative parameter, A_n, depends on the material viscosities (Brilliantov et al., 1996). It is computed by using a relation between the coefficient of restitution for the collision of two isolated particles and A_n by means of a Padé approximation (Schwager and Pöschel, 2008, 1998; Ramírez et al., 1999) — see Müller and Pöschel (2011) for a detailed description of the calculation method used in our simulations.

Furthermore, in Eq. (2), G is the shear modulus, which is given by the equation, $2G = Y/(1+\nu)$, while μ is the Coulomb friction coefficient. The integral in Eq. (2) is performed over the displacement of the colliding particles at the point of contact, for the total duration of the contact (Cundall and Strack, 1979). The relative tangential velocity at the point of contact is denoted by $\vec{v}_t = v_t \vec{e}_t$, with $\vec{e}_t$ standing for the corresponding unit vector. The tangential dissipative parameter, A_t, characterizes the surface roughness of the particles. It is chosen such that the prefactors of the normal and tangential deformation rates ($\dot{\xi}$ and $v_{\rm t}$) in Eqs. (1) and (2), respectively, are of the same order of magnitude (Schwager et al., 2008; Rycroft et al., 2009), which gives $A_t \approx A_n Y/(1-\nu^2)$.

In addition to contact forces, attractive particle interaction forces must be taken into account in order to simulate the dynamics of the powder particles. In our simulations, adhesion is taken into account via the JKR model (Johnson et al., 1971; Brilliantov et al., 2007; Barthel, 2008; Deng et al., 2013),

$$\vec{F}_{\rm JKR} = 4\sqrt{\frac{\pi a^3 \gamma Y}{2(1-\nu^2)}}\vec{e}_{\rm n}, \tag{5}$$

where γ is the surface energy density (Salmang and Scholze, 2007) and a is the contact radius, related to the deformation ξ through the equation

$$\xi = a^2/R_{\rm eff} - \sqrt{8(1-\nu^2)\pi a \gamma/Y}\,. \tag{6}$$

By rewritting Eq. (6) in the form (Deng et al., 2013),

$$a^4 - [2R_{\rm eff}\xi]a^2 - \left[8\left(1-\nu^2\right)\pi\gamma R_{\rm eff}^2/Y\right]a + \left[R_{\rm eff}^2\xi^2\right] = 0, \tag{7}$$

an expression is obtained which can be used to compute the contact radius a analytically as a function of the deformation ξ (Parteli et al., 2014).

Moreover, as shown previously (Yu et al., 1997; Parteli et al., 2014), non-bonded van-der-Waals interaction force may have a non-negligible influence on the dynamics of the powder system. It is given by (Hamaker, 1937; Eggersdorfer et al., 2010),

$$\vec{F}_{\rm vdW} = \begin{cases} \dfrac{A_H R_{\rm eff}}{6D_{\rm min}^2}\vec{e}_n & \text{if } \xi > 0, \\ \dfrac{A_H R_{\rm eff}}{6\left(\xi - D_{\rm min}\right)^2}\vec{e}_n & \text{if } -D_{\rm max} \le \xi \le 0 \\ 0, & \text{if } \xi < -D_{\rm max}\,, \end{cases} \tag{8}$$

where ξ is given by Eq. (3), while the Hamaker constant A_H is given by (Götzinger and Peukert, 2003),

$$A_H = 24\,\pi D_{\rm min}^2 \gamma. \tag{9}$$

In Eq. (8), $D_{\rm min} = 1.65\text{Å} = 1.65\times10^{-10}\,\text{m}$ is a parameter introduced to avoid the singularity of the Hamaker equation at $\xi = 0$ (Israelachvili, 1998; Götzinger and Peukert, 2003) and $D_{\rm max} = 1\,\mu\text{m}$ is the maximal (cutoff) distance of the van-der-Waals interaction (Parteli et al., 2014).

2.3. Numerical integration and model parameters

The integration is performed using the open-source library for DEM simulations developed by Kloss et al. (2012) (LIGGGHTS), which has been extended here in order to account for the particle model described above. Specifically, we have implemented in this DEM library the adhesion and non-bonded van-der-Waals forces (Eqs. (5) and (8)); the computation of the inertial properties of the complex particles (Parteli, 2013), and the model developed by Müller and Pöschel (2011) to compute the dissipative constant A_n of the viscoelastic force model as a function of the material parameters (see Eq. (1)).

The numerical values of the model parameters are given in Tab. 1. Note that the particle material density is consistent with the one for thermoplastic materials, but the Young's modulus used in the simulations — and thus the value of the elastic part of the contact force — is two orders of magnitude smaller than the real value (about 2.3 GPa (Amado-Becker et al., 2008)). This is because the computational time required for a DEM simulation decreases substantially by decreasing the value of Y. Accordingly, in order to maintain the ratio Y/A_H approximately the same, the Hamaker constant A_H used in our simulations is also two orders of magnitude smaller than the real value (20 zJ (Amado-Becker et al., 2008; Pegel et al., 2012)). From the value of A_H, the surface energy density γ is computed using Eq. (9).

Table 1: Numerical values of the parameters used in the simulations.

parameter	symbol	value
particle material density		$1000\,\text{kg/m}^3$
Young's modulus	Y	$2.3\times10^7\,\text{Pa}$
Poisson's ratio	ν	0.40
Coulomb's friction coefficient	μ	0.50
surface energy density	γ	$0.1\,\text{mJ/m}^2$
Hamaker constant	A_H	$0.2\times10^{-21}\text{J}$

The particle size distribution is consistent with the size distribution of commercially available PA12 powder (see Fig. 1c). Moreover, the integration time step Δt must be chosen small enough to correctly compute the particle interactions (Schäfer et al., 1996). Here we take Δt about an order of magnitude smaller than the collision time T_{col} associated with the smallest bead in a multisphere particle occurring in the simulation, which has a diameter 1.54 μm. The duration T_{col} of the collision can be estimated using the equation (Schäfer et al., 1996),

$$T_{\text{col}} \approx 3.21 \left(M_{\text{eff}}/\rho\right)^{2/5} \cdot v_{\text{imp}}^{-1/5}, \tag{10}$$

which is valid for undamped, non-adhesive collisions ($A_n = \gamma = 0$). In this equation, v_{imp} denotes a reference impact velocity and $M_{\text{eff}} = m_1 m_2/(m_1 + m_2)$ is the effective mass associated with the colliding particles, which have masses m_1 and m_2. Using $v_{\text{imp}} = 1.0\,\text{m/s}$ and the parameters mentioned above, we obtain $T_{\text{col}} \approx 7.5 \times 10^{-8}\,\text{s}$, and thus we take $\Delta t \approx 10^{-8}\,\text{s}$.

In our simulations, the dynamic boundary conditions associated with the complex geometry of the device's walls are taken explicitly into account. By using the interface to CAD programs that is implemented in the DEM library employed in our simulations (Kloss et al., 2012), triangular meshes can be imported and interpreted as frictional walls for the granular particles. The equations used for calculating the interaction forces between the powder particles and the frictional walls constituting the device geometry are the same used for modeling particle-particle collisions, with one of the contact partners being of infinite mass and radius (Parteli et al., 2014).

3. Simulation of the powder application

The coating device is a roller of diameter 2.5 mm, which moves from left to right in Fig. 2 thereby rotating in the counter-clockwise direction. In the simulations, periodic boundary conditions are used in the horizontal direction perpendicular to the transport (the y direction). Therefore, a longitudinal cut away from the lateral boundaries of the system comprising device, coating system and powder bed is modeled. The width of this cut, that is, the lateral dimension of the simulation volume in the direction perpendicular to the transport, is 400 μm. Vertical rough walls (not shown) are placed on both left and right ends of the powder bed, such that the total length of the volume containing the powder is about 4.5 mm.

We perform simulations with 5761 complex particles, modeled with the multisphere method and with the shapes shown in Fig. 1b, comprising a total of 24771 constituent spheres. Initially, the volume on both sides of the part is filled with powder particles and the surface of the part is free of powder. The powder particles are transported by the roller onto the surface of the part, which is represented by the green obstacle in the figure, approximated with the multisphere method, and has length (in the transport direction) of about 1 mm.

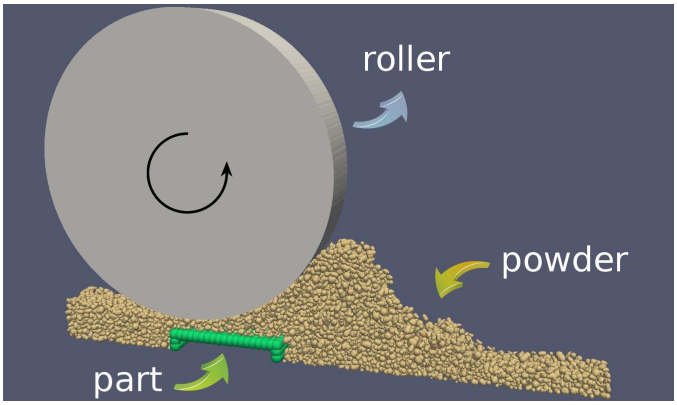

Figure 2: Snapshot of the simulation indicating the main elements of the powder application process. The roller moves from left to right thereby rotating in the counter-clockwise direction. Periodic boundary conditions are applied in the horizontal direction perpendicular to the transport, while particle motion is constrained by the presence of rough vertical walls (not shown) on the left and right ends of the simulation area.

Fig. 3 (top) shows one snapshot of the simulation with the particles color-coded by the magnitude of the total force due to the interaction with the other particles, the part and the walls of the device. The same color-coding is applied to the mesh elements composing the roller's axial wall. As we can see in this figure, a few particles in the powder carry large force values whereas most particles are associated with much lower load. This strongly inhomogeneous behavior of the load in granular packings is a well-known phenomenon that is due to the formation of force chains in the particulate system. As explained previously, the origin of these chains is the nearly point-like nature of the inter-particle contacts, which leads to the emergence of groups of particles through which most of the stress is transmitted (Liu et al., 1995; Hidalgo et al., 2004; Pöschel and Schwager, 2005). Particles in the zones between these chains are shielded for the effect of the particles constituting the chains, thus being subjected to lower stress.

Due to the dynamics of force chains in the packing, there are strong spatial and temporal fluctuations in the forces exerted by the granular material on the coating system and the part that is being built. Indeed, it can be seen in the snapshot of Fig. 3 (top) that the forces on the mesh elements of the roller's walls are quite inhomogeneously distributed. Moreover, the plot in Fig. 3 (bottom) shows the evolution of the magnitude of the components of the total force on the part in the horizontal and vertical directions (F_x and F_z, respectively), as a function of time. In the plot, the time is represented by the position of the roller as it moves in the transport direction and applies the powder onto the part — the corresponding snapshots are shown on top of the plot. As we can see, both com-

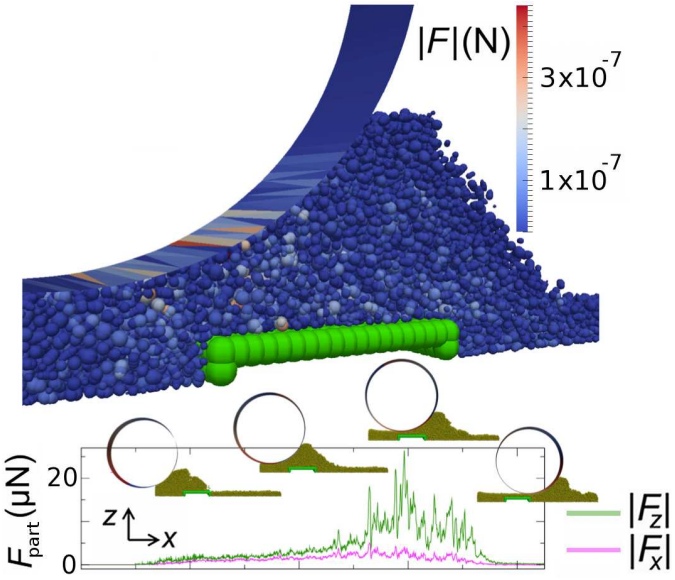

Figure 3: Snapshots of the powder application process onto the part (in green). In the snapshot on top, the powder particles, as well as the mesh elements composing the roller geometry, are color-coded by the magnitude of the total forces due to the interaction with their neighbouring particles (including contact and cohesive forces). Bottom: Magnitude of the vertical and horizontal components (F_z and F_x, respectively) of the total force F_{part} exerted by the granular particles on the part as a function of time — which is quantified by the position of the roller relative to the part in the snapshots along the horizontal axis.

ponents of the forces display strong variations in time. In particular, as the roller moves above the part, the vertical component of the total force on the part may vary within almost one order of magnitude. Clearly, our simulations display the ability to quantitatively assess the spatial and temporal evolution of the load in the powder bed. To the best of our knowledge, this is the first particle-based investigation of the load behavior on powder particles during powder application in additive manufacturing. The understanding of this behavior is important pre-requisite for modeling abrasion, plastic deformation and ageing of the material used in the production processes.

One fundamental aspect in the manufacturing process is to obtain homogeneous distribution of the powder material on the part. As a matter of fact, the surface of the deposited bed is typically far from being flat and may display many undulations (or ripples). This behavior, which is due to the poor flowability of the cohesive material used in the manufacturing process, may lead to low part densities and the occurrence of deffects both at the interior as well as at the surface of the part produced after the melting process. It is thus desirable to avoid this inhomogeneous packing behavior, which is challenging especially considering the low powder layer thickness that is typically deposited.

It is thus necessary to understand how the process dynamics affect the packing behavior of the powder bed *at the particle level*. This is important because the global packing properties of particulate ensembles are largely dictated by local packing characteristics, which in the case of powder layer formation in additive manufacturing are very difficult to assess experimentally. We thus apply our numerical tool to perform the first investigation of this behavior, using DEM simulations. Specifically, we perform simulations of the powder application using different velocities of the coating system in order to investigate how the production speed affects the powder layer.

Fig. 4 shows snapshots of the powder bed after deposition by the roller for two values of the translational velocity V_{R} (20 mm/s and 180 mm/s), which are well within the values typically employed in the production process (see e.g. Hoeges et al. (2010)). In the snapshots on top, the side view of the granular layer is shown (the left and right snapshots are for $V_{\text{R}} = 20$ mm/s and $V_{\text{R}} = 180$ mm/s, respectively), while the top view of each packing is shown in the bottom layer.

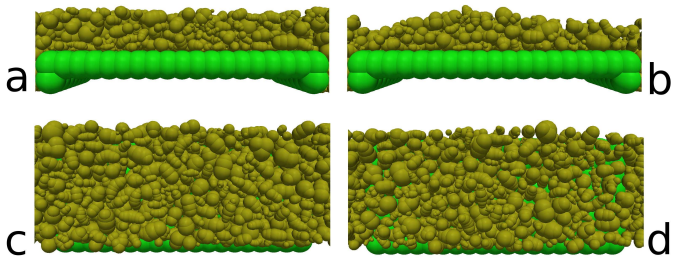

Figure 4: Powder layer applied onto the part to be built (green). (a) and (b) denote the side views of the powder layer obtained with $V_{\text{R}} = 20$ mm/s and 180 mm/s, respectively; (c) and (d) are the top views of the particles, again for $V_{\text{R}} = 20$ mm/s and 180 mm/s, respectively.

From Fig. 4, it is clear that a higher process speed leads to a looser packing, with the occurrence of larger voids between the particles and also a surface with larger undulations. This result can be understood by noting that the higher the velocity of the roller the more difficult it is for the particles to fill the voids that form during the transport thus leading to a higher packing fraction.

In order to quantitatively describe the topography of the powder bed, we compute the surface roughness δ of the particles, which is defined as the standard deviation of the height profile of the powder bed's cutout — its projection onto the vertical plane parallel to the transport direction. The dependence of the surface roughness δ on the coating velocity V_{R} is shown in the main plot of Fig. 5, in which simulation results are denoted by the filled circles. We see that the bed roughness increases monotonously with the coating speed. The continuous line in this plot denotes the best fit to the simulation data using a quadratic equation,

$$\delta(V_{\text{R}}) \approx a + b\,|V_{\text{R}}|^2, \tag{11}$$

which gives with $a \approx 6.05\,\mu$m and $b \approx 0.00039\,\mu$m, with δ in μm and V_{R} in mm/s. As we can see, this expression

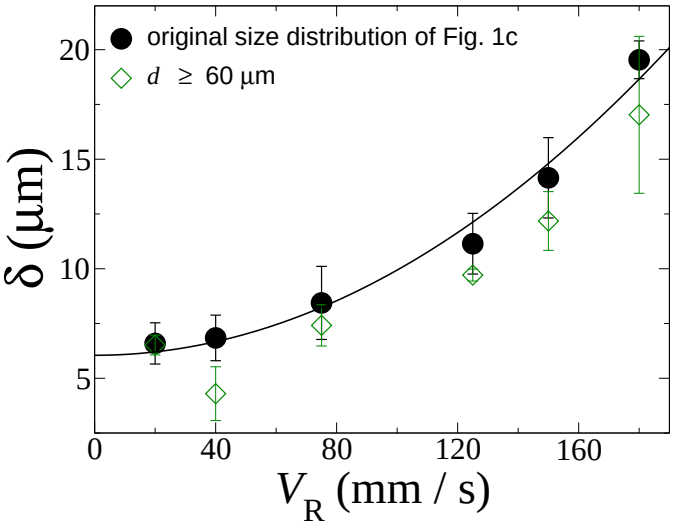

Figure 5: The filled symbols denote the roughness δ of the powder layer deposited on the part as a function translational velocity of the roller (V_{R}), for a constant roller's rotational velocity of 165 rpm. Error bars stem from an average over 3 longitudinal slices of the powder, each of width $L_y/3$, where $L_y = 400\,\mu$m is the width of the system in the transverse direction. The continuous line denotes the best fit to the data using Eq. (11), which gives $a \approx 6.05\,\mu$m and $b \approx 0.00039\,\mu$m. The empty diamonds denote simulation results for the modified version of the size distribution of Fig. 1c, after removing all particles smaller than $60\,\mu$m.

captures quantitatively well the behavior of the surface roughness with the roller's velocity. However, obviously the values of the fit parameters are not universal since they depend fundamentally on the material properties and the geometric characteristics of the coating system, and thus further research is needed in order to elucidate the role of material and process parameters on the packing characteristics. Nevertheless, the results of our simulations suggest that measures of process optimization based on increasing the coating speed alone may cause a decrease in particle distribution homogeneity and, consequently, a reduction in part quality — that is, in terms of production efficiency and quality, faster may not be better. To the best of our knowledge, there is no experimental investigation of the surface roughness as a function of V_{R}, which could be used to confirm our findings. However, that process speed can negatively affect the homogeneity of the deposited powder layer in additive manufacturing has been clearly shown in previous experimental investigations — for instance for the case of powder lines deposited by a nozzle (Stichel et al., 2013).

Moreover, is it possible to modify the packing characteristics by changing the particle size distribution of the applied powder? In order to address this question, here we perform simulations with the same powder particles modeled with Fig. 1, but with a different size distribution. Specifically, we remove from the size distribution of Fig. 1c all particles with diameter smaller than $60\,\mu$m, and perform simulations using the same volume of powder as before. We obtain a surprising result. Even though the particles of this new distribution are much coarser than in the original powder, the values of surface roughness for the modified powder are *smaller* than for the original one (cf. Fig. 5).

This result is, indeed, unexpected because it is known that in an agitated polydisperse granular bed, small particles tend to fill the voids between the big particles, thus contributing to decrease the porosity of the packing (Pöschel and Schwager, 2005). However, for powders the situation may be very different since the smallest particles are most prone to form large agglomerates due to the increased relevance of attractive particle interaction forces, relative to particle weight (Yu et al., 1997; Parteli et al., 2014). Indeed, it was recently shown, both experimentally and by means of DEM simulations, that the porosity of fine powders *increases* with decreasing particle size (Parteli et al., 2014). Due to the strong attractive particle interactions, the small particles are transported as large agglomerates of irregular shapes and different volumes, rather than flowing as single particles. Consequently, as the roller moves over the part, the surface roughness of the applied powder is largely affected by the shape and size characteristics of the particle agglomerates, and thus by the particle size distribution.

Our simulations should be now extended in order to investigate how the results presented here change when a vertical pressure is exerted by the roller on the powder, as well as by considering more realistic boundary conditions associated with the part (e.g. to include viscosity associated with the molten polymeric particles). However, the present study clearly shows that it is possible to achieve determined powder layer characteristics by tuning not only process parameters like the roller's speed but also by modifying the particle size distribution of the applied powder.

4. Conclusions

We developed a numerical tool for particle-based simulations of powder application in additive manufacturing devices under consideration of complex particle geometric shapes. We applied our model to investigate the transport of powder particles using a roller as coating system, and we found that the process speed plays an important role for the packing characteristics of the applied powder. Specifically, our simulations predict a quadratic scaling of surface roughness of the powder bed deposited onto the part with the roller velocity. Moreover, we have also found that a strong polydispersity may lead to larger surface roughness due to the tendency of very small particles to form large agglomerates as a result of attractive particle interaction forces. Finally, we have also shown that the temporal evolution of the force exerted by the granular material on the part during the transport process is characterized by strong fluctuations, owing to the dynamics of force chains that are inherent to granular materials.

Our model should be now extended in order to include electrostatic interactions, which could play an important role for the dynamics of powder systems (Matsusaka et al., 2010). This modeling should account not only for the long-range Coulomb interactions between charged particles but also for the complex — and still poorly understood — mechanism of tribocharging. Considering the many complex types of inter-particle forces and particle shapes, the Discrete Element Method provides an indispensable tool in the investigation of the influence that particle characteristics and interactions have on the (macroscopic) mechanical behavior of the bulk.

The future application of our numerical tool may be helpful for developing optimization strategies for process and particle characteristics with regard to packing behavior and flowability of the applied powder. For instance, how do geometry and surface texture of the coating device influence the porosity and surface roughness of the deposited powder layer? Moreover, how could mechanical vibrations be applied to the system in order to achieve size segregation or compaction in the powder bed? Is it possible to obtain prescribed gradation properties in the powder bed by suitably designing the dynamic boundary conditions (coating system, vibrations) and mixing powder systems of different shape and size distributions? These are a few examples of a broad range of questions that call for particle-based simulations of the application process, and which we shall address in the future by applying the numerical simulation tool presented in this work.

Acknowledgments

We thank Maximilian Drexler and Katrin Wudy for providing us with the particle size distribution and light microscope images of the commercially available PA12 powder. We thank the German Research Foundation (DFG) for funding through the Cluster of Excellence "Engineering of Advanced Materials" and through the Collaborative Research Initiative "Additive Manufacturing" (SFB814). The authors gratefully acknowledge the computing time granted by the John von Neumann Institute for Computing (NIC) and provided on the supercomputer JUROPA at Jülich Supercomputing Centre (JSC).

References

Abdel Ghany, K., Moustafa, S. F., 2006. Comparison between the products of four rpm systems for metals. Rapid Prototyping J. 12, 86–94.

Amado-Becker, A., Ramos-Grez, J., Yañez, M. J., Vargas, Y., Gaete, L., 2008. Elastic tensor stiffness coefficients for SLS Nylon 12 under different degrees of densification as measured by ultrasonic technique. Rapid Prototyping J. 14, 260–270.

Barthel, E., 2008. Adhesive elastic contacts: JKR and more. J. Phys. D.: Appl. Phys. 41, 163001.

Brilliantov, N. V., Albers, N., Spahn, F., Pöschel, T., 2007. Collision dynamics of granular particles with adhesion. Phys. Rev. E 76, 051302.

Brilliantov, N. V., Spahn, F., Hertzsch, J.-M., Pöschel, T., 1996. A model for collision in granular gases. Phys. Rev. E 53, 5382–5392.

Campbell, I., Bourell, D., Gibson, I., 2012. Additive manufacturing: rapid prototyping comes of age. Rapid Prototyping J. 18, 255–258.

Cundall, P. A., Strack, O. D. L., 1979. A discrete numerical model for granular assemblies. Geotechnique 29, 47–65.

Deng, X. L., Scicolone, J. V., Davé, R. N., 2013. Discrete element method simulation of cohesive particles mixing under magnetically assisted impaction. Powder Technol. 243, 96–109.

Eggersdorfer, M. L., Kadau, D., Herrmann, H. J., Pratsinis, S. E., 2010. Fragmentation and restructuring of soft-agglomerates under shear. J. Colloid Interface Sci. 342, 261–268.

Ferellec, J. F., McDowell, G. R., 2010. A method to model realistic particle shape and inertia in dem. Granular Matter 12, 459–467.

Gallas, J. A. C., Sokołowski, S., 1993. Grain non-sphericity effects on the angle of repose of granular material. Int. J. Mod. Phys. 7, 2037–2046.

Garcia, X., Latham, J. P., Xiang, J., Harrison, J. P., 2009. A clustered overlapping sphere algorithm to represent real particles in discrete element modelling. Géotechnique 59, 779–784.

Goodridge, R. D., Tuck, C. J., Hague, R. J. M., 2012. Laser sintering of polyamides and other polymers. Prog. Mater. Sci. 57, 229–267.

Götzinger, M., Peukert, W., 2003. Dispersive forces of particle-surface interactions: direct AFM measurements and modelling. Powder Technology 130, 102–109.

Hamaker, H. C., 1937. The London-van der Waals Attraction Between Spherical Particles. Physica 4, 1058–1072.

Heinl, P., Rottmair, A., Körner, C., Singer, R. F., 2007. Cellular titanium by selective electron beam melting. Adv. Eng. Mater. 9, 360–364.

Herrmann, H. J., 1993. Molecular dynamics simulations of granular materials. Int. J. Mod. Phys. C 4, 309–316.

Hidalgo, R. C., Herrmann, H. J., Kun, F., Parteli, E. J. R., 2004. Force chains in granular packings. In: Mallamace, F., Stanley, H. (Eds.), The Physics of Complex Systems. IOS Press, Amsterdam, pp. 153–171.

Hoeges, S., Lindner, M., Meiners, W., Smeets, R., 2010. Bioresorbable Implants using Selective Laser Melting. In: Bourell, D. (Ed.), Proceedings of the Solid Freeform Fabrication Symposium (SFF). Austin, Texas, pp. 908–920.

Israelachvili, J., 1998. Intermolecular & Surface Forces. Academic Press, London.

Johnson, K. L., Kendall, K., Roberts, A. D., 1971. Surface energy and the contact of elastic solids. Proc. R. Soc. Lond. Ser. A Math. Phys. Sci. 324, 301–313.

Karunakaran, K. P., Bernard, A., Suryakumar, S., Dembinski, L., Taillandier, G., 2012. Rapid manufacturing of metallic objects. Rapid Prototyping J. 18, 264–280.

Kloss, C., Goniva, C., Hager, A., Amberger, S., Pirker, S., 2012. Models, algorithms and validation for opensource DEM and CFD-DEM. Prog. Comput. Fluid Dy. 12, 140–152, `http://www.liggghts.com`.

Kruggel-Emden, H., Simsek, E., Rickelt, S., Wirtz, S., Scherer, V., 2007. Review and extension of normal force models for the Discrete Element Method. Powder Technol. 171, 157–173.

Kruggel-Emden, H., Wirtz, S., Scherer, V., 2008. A study on tangential force laws applicable to the discrete element method (DEM) for materials with viscoelastic or plastic behavior. Chem. Eng. Sci. 63, 1523–1541.

Liu, C. H., Nagel, S. R., Schecter, D. A., Coppersmith, S. N., Majumdar, S., Narayan, O., Witten, T. A., 1995. Force fluctuations in bead packs. Science 269, 513–515.

Matsusaka, S., Maruyama, H., Matsuyama, T., Ghadiri, M., 2010. Triboelectric charging of powders: A review. Chemical Engineering Science 22, 5781–5807.

Müller, P., Pöschel, T., 2011. Collision of viscoelastic sphere: Compact expressions for the coefficient of normal restitution. Phys. Rev. E 84, 021302.

Parteli, E. J. R., 2013. DEM simulation of particles of complex shapes using the multisphere method: Application for additive manufacturing. AIP Conf. Proc. 1542, 185–188.

Parteli, E. J. R., Schmidt, J., Blümel, C., Wirth, K.-E., Peukert, W., Pöschel, T., 2014. Attractive particle interaction forces and packing density of fine glass powders. Scientific Reports 4, 6227.

Pegel, S., Villmow, T., Kasaliwal, G., Pötschke, P., 2012. Polymer-carbon nanotube composites: Melt processing, properties and applications. In: Fakirov, D. B. (Ed.), Synthetic Polymer-Polymer Composites. Hanser, pp. 145 – 191.

Pöschel, T., Buchholtz, V., 1993. Static friction phenomena in granular materials: Coulomb law versu s particle geometry. Phys. Rev. Lett. 71, 3964–3966.

Pöschel, T., Schwager, T., 2005. Computational Granular Dynamics. Springer, Heidelberg.

Ramírez, R., Pöschel, T., Brilliantov, N. V., Schwager, T., 1999. Coefficient of restitution of colliding viscoelastic spheres. Phys. Rev. E 60, 4465–4472.

Rietzel, D., Kühnlein, D., Drummer, D., 2011. Selektives Lasersintern von teilkristallinen Thermoplasten. RTejournal - Forum für Rapid Technologie 6, urn:nbn:de:0009–2–31138.

Rycroft, C. H., Orpe, A. V., Kudrolli, A., 2009. Physical test of a particle simulation model in a sheared granular system. Phys. Rev. E 80, 031035.

Salmang, H., Scholze, H., 2007. Keramik. Springer, Heidelberg.

Schäfer, J., Dippel, S., Wolf, D. E., 1996. Force Schemes in Simulations of Granular Materials. J. Phys. I France 6, 5–20.

Schwager, T., Becker, V., Pöschel, T., 2008. Coefficient of tangential restitution for viscoelastic spheres. Eur. Phys. J. E 27, 107–114.

Schwager, T., Pöschel, T., 1998. Coefficient of restitution of viscous particles and cooling rate of granular gases. Phys. Rev. E 57, 650–654.

Schwager, T., Pöschel, T., 2008. Coefficient of restitution for viscoelastic spheres: The effect of delayed recovery. Phys. Rev. E 78, 051304.

Silbert, L. E., Ertaş, D., Grest, G. S., Halsey, T. C., Levine, D., Plimpton, S. J., 2001. Granular flow down an inclined plane: Bagnold scaling and rheology. Phys. Rev. E 64, 051302.

Stichel, T., Laumer, T., Baumüller, T., Amend, P., Schmidt, M., 2013. Polymer powder deposition with vibrating capillary nozzles for additive manufacturing. In: Proceedings of the Polymer Processing Society 29th Annual Meeting - PPS-29. Nuremberg, Germany.

Wendel, B., Rietzel, D., Kühlein, F., Feulner, R., Hülder, G., Schmachtenberg, E., 2008. Additive processing of polymers. Macromol. Mater. Eng. 293, 799–809.

Wudy, K., Drummer, D., Drexler, M., 2014. Characterization of polymer materials and powders for selective laser melting. AIP Conf. Proc. 1593, 702–707.

Yu, A. B., Bridgwater, J., Burbidge, A., 1997. On the modelling of the packing of fine particles. Powder Technol. 92, 185–194.

Zhang, H. P., Makse, H. A., 2005. Jamming transition in emulsions and granular materials. Phys. Rev. E 72, 011301.